# The intriguing role of collagen on the rheology of cancer cell spheroids

Daria Tsvirkun, Jean Revilloud, Arianna Giannetti, Claude Verdier

# The intriguing role of collagen on the rheology of cancer cell spheroids

Daria Tsvirkun[a], Jean Revilloud[a], Arianna Giannetti[a], Claude Verdier[1 a]

[a] *Université Grenoble Alpes, CNRS, LIPhy, Grenoble, 38000, France*

**Abstract**

Spheroids are multicellular systems with an interesting rheology giving rise to elasto–visco–plastic properties. They are good tumor models, but the role of the extracellular matrix (ECM) is not fully understood. ECM is an important link between cells and may have a significant impact on tissue organization. Here we determine viscoelastic properties of spheroids including different collagen I amounts using AFM and predict new frequency–dependent properties leading to soft glassy rheology behavior. A unified model – similar to single cell behavior – is proposed and discussed, while complementary confocal experiments reveal the microstructure of spheroids, with collagen I fibers serving as a skeleton for cells, thus reinforcing the spheroid viscoelastic behavior.

*Keywords:* cancer cells, collagen, spheroids, viscoelastic, confocal microscopy, AFM,

*PACS:* 87.15.La, 87.18.Ed, 87.19.xj

*2000 MSC:* 74L15, 92C10, 74D05

[1] claude.verdier@univ-grenoble-alpes.fr

## 1. Introduction

While the mechanical properties of cancer cells have been extensively studied (Lekka et al. (1999); Cross et al. (2007); Rother et al. (2014); Abidine et al. (2015); Yubero et al. (2020)), the tissue scale remains less explored (Plodinec et al. (2012)); therefore it is important to understand how cellular properties combine together and whether the local rheology is retained at a higher scale.

Tissues are usually made of cells surrounded by the extracellular matrix (ECM) inside a fluid (Fung (1993)), so that concentrations of the different components are important to characterize the full tissue. In particular the amount of fluid may give rise to rate–dependent properties. As for the ECM behaving usually as a physical gel, its rheology is well represented by a viscoelastic behavior. Concentrated cell suspensions (volume concentration around 50%) have been considered using mixture models and exhibit viscoplastic behaviors (Iordan et al. (2008); Preziosi et al. (2010)). Biological tissues containing nanofibres may be modeled as elasto-plastic materials, with only a few heterogeneities enough to generate such plastic effects (Groetsch et al. (2021)). On the other hand, with a large collagen content and a small amount of cells (around 10%), the behavior becomes viscoelastic (Iordan et al. (2010)), but the interactions between cells and the ECM are essential, since cells can remodel the collagen network and change tissue properties. Here we study tissue models containing a large number of cells with small amounts of ECM within culture medium. To investigate such biological tissues, in particular solid tumors, multicellular spheroids have been developed over the years (Netti et al. (1996); Delarue et al. (2013); Weiswald et al. (2015)) and appear as outstanding *in vitro* models in cancer research. They are made of cells grown

in culture medium until they are closely packed together. Cells within spheroids can produce their own ECM, and express cell adhesion molecules (e.g. cadherins) to bind together.

With regard to *in vivo* tumors, the amount of ECM or collagen is not so well quantified but the microenvironment affects cancer cell motility a lot, and serves as a guide, especially when cells contract to align collagen fibers (Levental et al. (2007); Mierke (2019)). Furthermore the interactions between collagen–rich tissues at the tumor–stromal boundary can be an important cause of tumorigenesis and invasion (Provenzano et al. (2006); Kai et al. (2019)), since collagen structures polymerize around cells and form bundles or wavy structures (Natarajan et al. (2019)). A negative correlation between patient survival and collagen I (Col-I) deposition was found (Whatcott et al. (2015)). In non-muscle invasive bladder cancers, the high Col-I expression was associated with tumor progression and poor prognosis (Brooks et al. (2016)). This is why collagen can be considered as a potential tool for tumor therapy due its strong interactions with cancer cells (Quarto et al. (2014); Xu et al. (2019)).

Several earlier studies focused on the role of compressive stresses (mechanical or osmotic) exerted by the outside onto the tumor (Helmlinger et al. (1997)) or spheroid (Delarue et al. (2014)), leading to limited growth. Fewer results are devoted to the mechanical behavior of such spheroids (Marmottant et al. (2009)), or measuring static AFM data (Ouchi et al. (2019); Tietze et al. (2019)). Some models focused on the flow of interstitial liquid within the spheroids (Netti et al. (1996); Delarue et al. (2013)) revealing that poroelastic active models can fully describe them (Dolega et al. (2021)). Time is therefore an essential parameter, so it is important to study frequency–dependent properties, i.e. viscoelastic ones. Such effects, already observed on cartilage or tendons, revealed notable high-frequency poroelastic responses (Nia et al. (2013); Connizzo and Grodzinsky (2017))

to differentiate physiological and pathological tissues.

In this work, AFM was chosen as an interesting approach to probe spheroids, made of bladder cancer cells in Col-I matrix. Data covering three decades in frequency was obtained and fitted with a relevant rheological model. Complementary confocal microscopy experiments allowed to highlight the role of Col-I, enhancing the viscoelastic properties.

## 2. Methods

### *2.1. Multicellular spheroids preparation*

We used T24 epithelial bladder cancer cells (ATCC, HTB–4, Manassas, VA). These cells are poorly differentiated and highly invasive. T24 cells were cultured in RPMI 1640 (Gibco, Saint-Aubin, France) supplemented with 10% (v/v) fetal bovine serum (FBS, Life Technologies SAS, Villebon-sur-Yvette, France) and 1% (v/v) penicillin-streptomycin solution (Life Technologies SAS). Cells have been stably transfected with a plasmid expressing LifeAct–GFP to stain F–actin (Riedl et al. (2008)). Cells were stored at 37°C in a humidified atmosphere and 5% $CO_2$.

We chose a method based on spheroid production in hanging drops (Kuo et al. (2017)). The Petri dish cover part was coated with a PDMS layer (w/w mixture of Stilgar PDMS 9/10 and crosslinker 1/10, baked at 60°C for 2 hours). PDMS can hold microscale drops without cellular adhesion even in the presence of extracellular matrix molecules. To form hanging drops, a T24 cell suspension was mixed with Col-I rat tail (Corning, Bedford, MA, USA) in culture medium at 4°C and pH ~ 7.4, at Col-I concentrations ($c_0$) of 0, 0.01 and 0.03 mg/mL. Cellular drops of 15 $\mu$L containing 5,000 cells each were dispensed on the PDMS surface (Figure 1). The cover part with drops was flipped onto the Petri dish lower part, filled with DPBS to avoid drying of drops, and

kept for three days at 37°C in a humidified atmosphere and 5% $CO_2$.

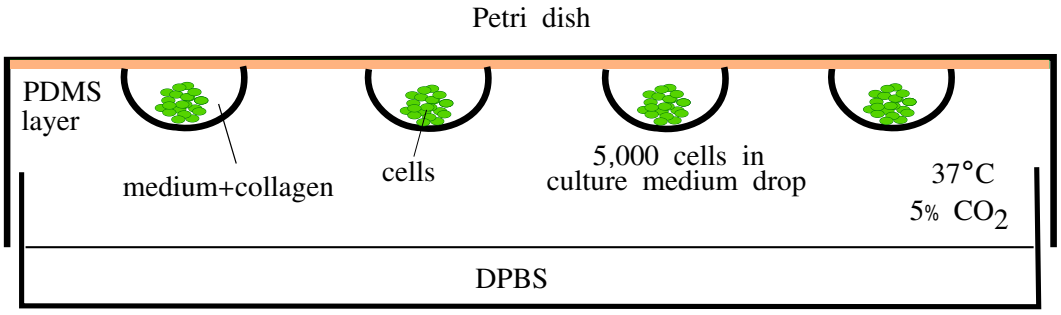


Figure 1: Preparation of spheroids: 15 $\mu$L drops containing 5,000 cells (green) in culture medium with (or without) Col-I are laid in the Petri dish cover (pretreated with a PDMS layer) which is eventually flipped onto the lower part, so that spheroids can form and do not adhere to the top of the Petri dish.

Cells remained at the bottom of the droplet and aggregated in time. After 3 days, aggregates usually presented a spherical, compact shape (diameter between 200 and 350 $\mu$m, Figure 2). Spheroids were caught using a chopped cone (200 $\mu$L) and deposited into a TPP Petri dish. After sedimentation and low adhesion to the dish, 2 mL culture medium (as above, with 1% HEPES) was poured gently around the spheroid and the Petri dish was set onto the AFM Petri dish heater (JPK, 37 ± 0.1 °C). The precalibrated AFM cantilever was then lowered to come into contact with the spheroid (Figure 3a). Measurements were carried out as explained below (Section 2.2).

### *2.2. AFM in force modulation*

AFM experiments were achieved using a Nanowizard II (JPK Instruments, Berlin) mounted on a Zeiss microscope (Observer D1) at 37°C. The AFM cantilever is usually set in contact with a surface to measure the interaction forces. Calibration was performed for the sensibility parameter ($s \sim$ 30–50 nm/V), then using thermal fluctuations (Butt and Jaschke (1995)) to obtain the can-

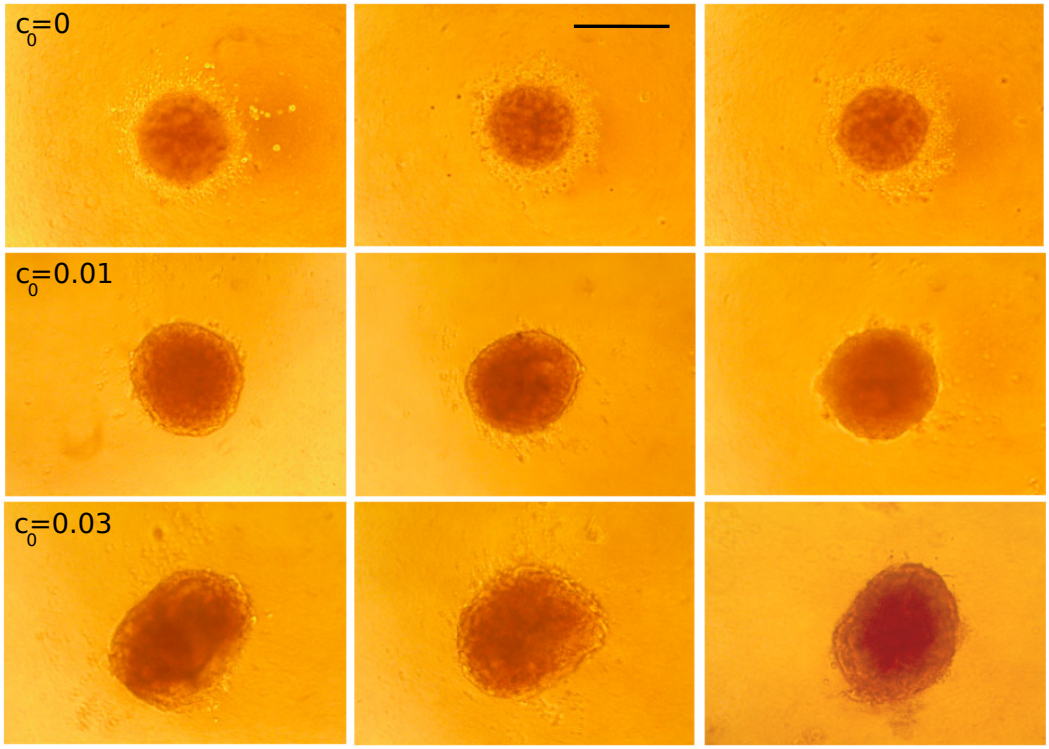


Figure 2: Role of Col-I concentration $c_0$ on spheroid size and microstructure. Three preparations are shown on each line for different Col-I concentrations. Top row: $c_0$ = 0 mg/mL, middle row: $c_0$ = 0.01 mg/mL, bottom row: $c_0$ = 0.03 mg/mL. Scale bar = 200 $\mu$m (same for all images).

tilever stiffness (k $\sim$ 30 N/m, stiff for large spheroid moduli). We performed an initial indentation $\delta_0$ (between 1 and 6 $\mu$m), then superimposed small sinusoidal deformations $\delta$ (small enough to remain in the linear viscoelastic range, typically $\delta \sim \delta_0/10$) in closed loop at a given frequency $f$.

An example is shown in Figure 3b, where the initial approach was followed by oscillation of the piezo at frequencies increasing from 1 to 32 Hz. Note that linear theory is verified since both piezo height Z(t) and force F(t) oscillate at the same frequency. The indentation was $\delta_0 = \Delta Z - F_0/\mathrm{k}$, where $\Delta Z$ is "piezo–height measured" change, $F_0$ is the applied force and the second term accounts for cantilever bending. In this case we found $\delta_0 \sim 1.2\,\mu$m. Large tipless cantilevers (Nanosensors,

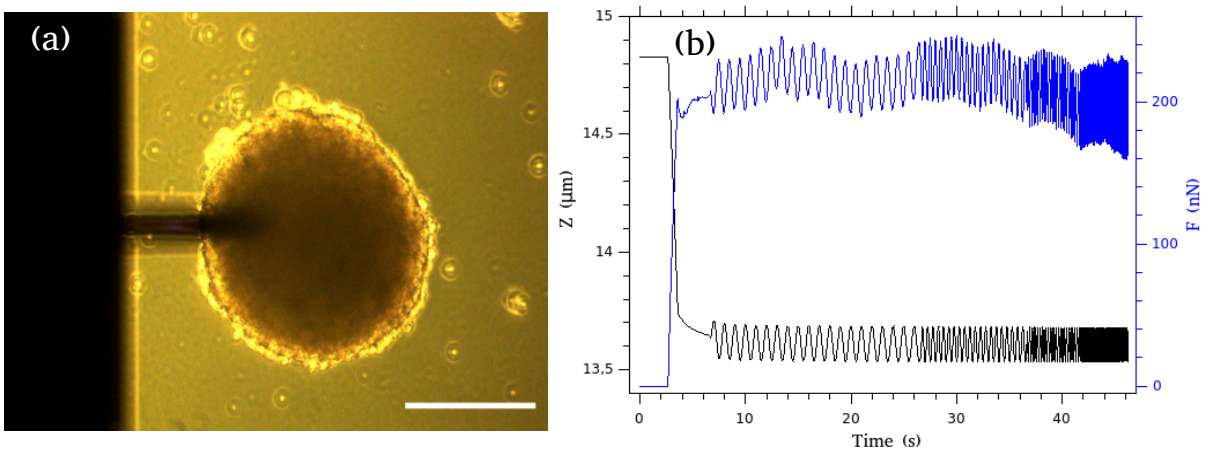


Figure 3: (a) Microscopy image of the AFM cantilever close to the top of the spheroid ($c_0$ = 0 mg/mL, R ~ 175 $\mu$m). Scale bar = 200 $\mu$m. (b) Typical applied piezo height $Z(t)$ (black) and measured $F(t)$ (blue), corresponding to the approach of the cantilever for an applied force $F_0$ = 200nN, relaxation for 4 s, followed by oscillations (amplitude $\delta$ of 0.07 $\mu$m) at 1 Hz, 2 Hz, 4 Hz, 8 Hz, 16 Hz, 32 Hz in this example. Piezo height $Z(t)$ and force $F(t)$ vary at the same frequency, but signals exhibit a phase shift. We use $\delta_0 = \Delta Z - F_0/k$. $\Delta Z = 1.2\mu$m can be checked from the graph, while the second term $F_0/k \sim 6.7$nm is negligible therefore $\delta_0 \sim 1.2\,\mu$m. Using Hertz equation $F_0 = \frac{4}{3}\frac{E\sqrt{R}\delta_0^{3/2}}{1-\nu^2}$, and the above values of $\delta_0$, $F_0$, R (measured), and $\nu \sim 0.5$, we deduce the static modulus E ~ 7.7kPa.

TL-NCL model, length 225 $\mu$m, width 38 $\mu$m, Giannetti et al. (2020)) were used to indent the spheroid with a maximum contact area (typically ~ 1200–5000 $\mu$m$^2$) but no buldging effect. The large contact area was necessary to solicit the whole spheroid. Hertz formula (inverse sphere-plane contact) relates the applied force $F_0$ to the indentation $\delta_0$: $F_0 = \frac{4}{3}\frac{E\sqrt{R}\delta_0^{3/2}}{1-\nu^2}$ where $E$ is the Young's spheroid modulus, $\nu$ its Poisson ratio ($\nu \sim 0.5$). R is the radius of the spheroid (in fact the radius of curvature, from Figure 3a, assuming it remains constant because small indentations are involved). From Figure 3b and the above data, Hertz formula gives the static Young modulus E = 7.7kPa. After linearizing and keeping only first order terms, one finds (Cai et al. (2013)):

$$G^*(\omega) = G' + i\,G" = \frac{1-\nu}{4\sqrt{R\delta_0}}\left\{\frac{F^*(\omega)}{\delta^*(\omega)} - i\,\omega b(0)\right\} \quad (1)$$

where $\omega$ is the angular frequency (rad/s) $\omega = 2\pi f$, $f$ being the frequency (Hz). $G'$ and $G''$ are respectively the elastic and viscous shear moduli. In Equation (1), the hydrodynamic drag was calibrated by oscillating the cantilever in the fluid (Alcaraz et al. (2002)). The drag is proportional to viscosity, velocity, depends on cantilever-to-surface distance $h$ through $b(h)$, which is obtained experimentally and extrapolated as h $\rightarrow$ 0. We found that b(0) = 3.45 $10^{-5}$ N.s/m.

### *2.3. Rheological model*

Different authors have modeled viscoelastic data, in particular studying polymers or complex materials (Palade et al. (1996); Sollich et al. (1997); Fabry et al. (2001)). For example, it was reported that cells have moduli ($G'$, $G''$) varying with a power–law exponent $\alpha \sim 0.1$–$0.3$ at low frequencies (Trepat et al. (2008); Alcaraz et al. (2003)), and could behave as Newtonian fluids (viscosity $\eta$) at larger frequencies, thus $G^*(\omega) = G\,(i\omega\tau)^\alpha + i\omega\eta$, where $\tau$ is a typical time scale, and $G$ is an elastic modulus. Sometimes a single exponent is not enough to cover the whole frequency range (Stamenovic et al. (2007); Abidine et al. (2015, 2018)). Our data suggested that one exponent only was enough for $G'$ whereas two exponents were necessary for $G''$:

$$G' = G_0\,(\frac{f}{f_0})^a\,, \qquad G'' = G_1\,(\frac{f}{f_0})^b + G_2\,(\frac{f}{f_0})^c \quad (2)$$

Letting $f_0 = 1$ Hz while $f$ is expressed in Hz allows to obtain prefactors $G_0, G_1, G_2$ in Pascals (Pa). Finally another possible criterion is to use the loss tangent $\frac{G''}{G'}$ (Rother et al. (2014)) which was found to be associated with the metastatic potential.

### 2.4. Confocal microscopy

Confocal imaging of spheroids produced in 0, 0.01 or 0.03 mg/mL Col-I was carried out using a Leica TCS SP8 confocal microscope. Cells expressing F-actin GFP were imaged in the green channel (argon laser, 488 nm), and Col-I was imaged using the reflectance technique (Friedl et al. (2001)) in the red channel (HeNe laser, 633 nm, Abidine et al. (2021)). Spheroids were allowed to settle in a Petri dish (with a glass coverslip at the bottom) at 37°C. They were imaged using a Leica APO 40×/1.30 Oil objective and Zoom ×0.75. Z-stacks were acquired using steps of 0.35 $\mu$m. For each image, 5 slices located at the mid–plane were projected to enhance intensity and reduce noise.

### 2.5. Statistics

Statistical analysis to compare the three cases was done using one–way ANOVA. At least $N > 10$ spheroids were measured. Statistical significance was reached for $^{*}p < 0.05$, $^{**}p < 0.01$, $^{***}p < 0.001$, while $p > 0.05$ was considered non significant. Means are presented together with the standard error of the mean (SEM).

## 3. Results

### 3.1. Rheology and modeling

Spheroids viscoelastic moduli $G'$ and $G''$ were measured in the [1–1024Hz] frequency range using frequencies that are multiples of 2. Results are shown in Figure 4. We also measured the static Young moduli ($E$) using indentation curves; results are reported in Table 1.

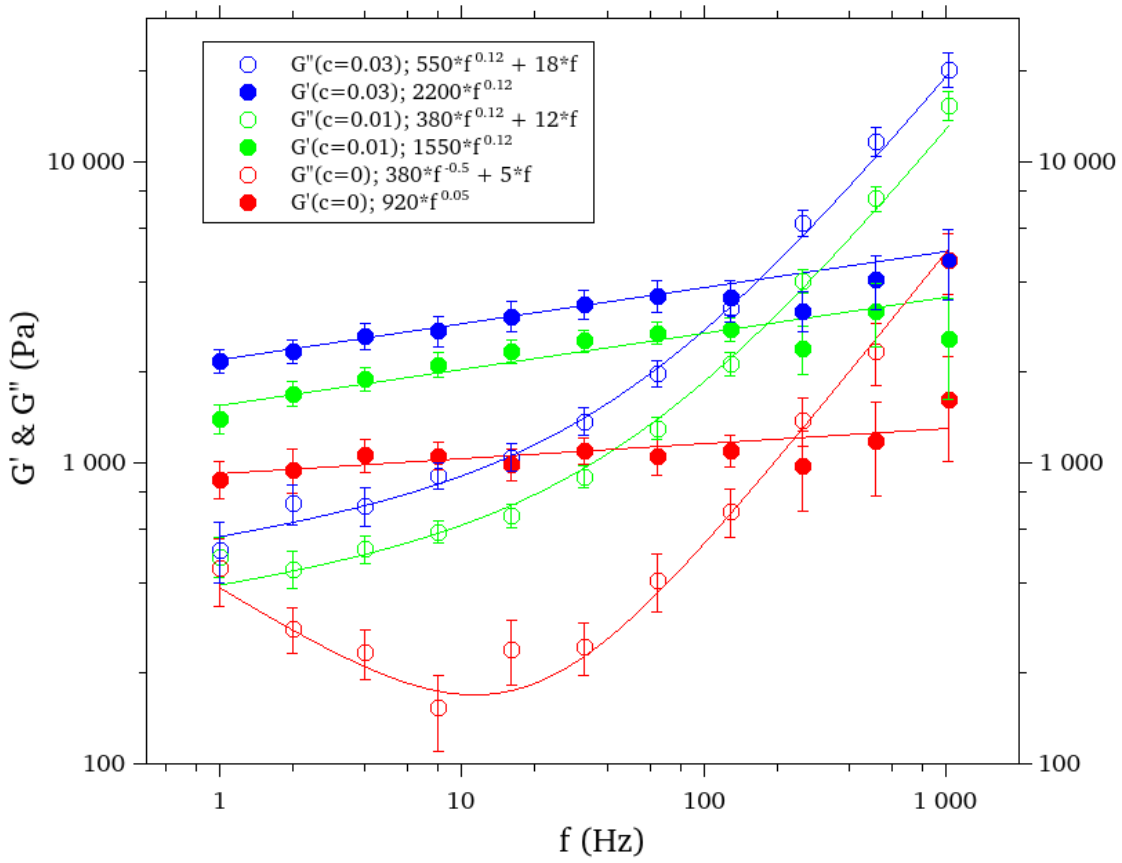


Figure 4: Viscoelastic moduli $G'$ (filled circles) and $G''$(empty circles) for Col-I concentrations $c_0 = 0$ (red, N=14), $c_0 = 0.01$ mg/mL (green, N=11), and $c_0 = 0.03$ mg/mL (blue, N=11). Fits obtained with the model are also provided in the legend. Error bars indicate mean value +/- SEM.

The data was averaged (N>10) and showed some intriguing effects due to the presence of the Col-I extra-cellular matrix. For all frequencies, power laws were found to fit $G'$. On the other hand, $G''$ exhibited two power–law exponents, one at low frequencies, and a slope of 1 at higher frequencies typical of a viscous behavior. Therefore the following fits $G' = G_0\, f^a$ and $G'' = G_1\, f^b + G_2\, f^c$ apply well (Figure 4) with parameters listed in Table 1. Such behaviors are similar to the ones obtained for the rheology of biological materials, with a possible minimum

| $c_0$ (mg/mL) | $E$ (Pa) | $G_0$ (Pa) | $G_1$ (Pa) | $G_2$ (Pa) | a | b | $c$ | $f_T$ (Hz) |
|---|---|---|---|---|---|---|---|---|
| 0 | 3100 | 920 | 380 | 5 | 0.05 | -0.5 | 1 | 197 |
| 0.01 | 3600 | 1550 | 380 | 12 | 0.12 | 0.12 | 1 | 182 |
| 0.03 | 5400 | 2200 | 550 | 18 | 0.12 | 0.12 | 1 | 170 |

Table 1: Parameters are defined by: $G' = G_0\, f^a$ and $G'' = G_1\, f^b + G_2\, f^c$, using $f_0$=1Hz, and $f$ (in Hz). Fitting was obtained using the mean values of $G'$ and $G''$ at each frequency. $f_T$ is the transition frequency corresponding to the crossing $G' = G''$. $E$ (Pa) is the static modulus, and $c_0$ is the Col-I concentration.

for $G''$, corresponding to the elastic plateau of $G'$ (Verdier et al. (2009)). Another parameter, the transition frequency $f_T$ – separating the elastic regime from the glassy behavior – is also indicated. It verifies $G'(f_T) = G''(f_T)$. We find decreasing transition frequencies ($f_T$ = 197 Hz, 182 Hz and 170 Hz) with increasing $c_0$.

Using the loss tangent $\frac{G''}{G'}$ (Rother et al. (2014)) can be interesting for spheroids with Col-I. Indeed, a=b=0.12 therefore $\frac{G''}{G'} = \frac{G_1}{G_0} + \frac{G_2}{G_0}\, f^{0.88}$ is an increasing function of the frequency. Further comparisons of the viscoelastic data can be made through simple statistics using moduli $G'$ and $G''$. For example at 8Hz, we compared moduli for different Col-I concentrations (Figure 5). This choice of frequency is arbitrary and other frequencies give similar results (data not shown). Moduli $G'$(8Hz) and $G''$(8Hz) for spheroids with Col-I are significantly different from spheroids without Col-I ($p<0.001$), and this also applies between $c_0$ = 0.01 mg/mL and $c_0$ = 0.03 mg/mL ($p<0.05$).

To summarize:

- $c_0$ = 0: the spheroids show a roughly constant $G' \sim 1000$ Pa (weak slope $a$ = 0.05). $G''$

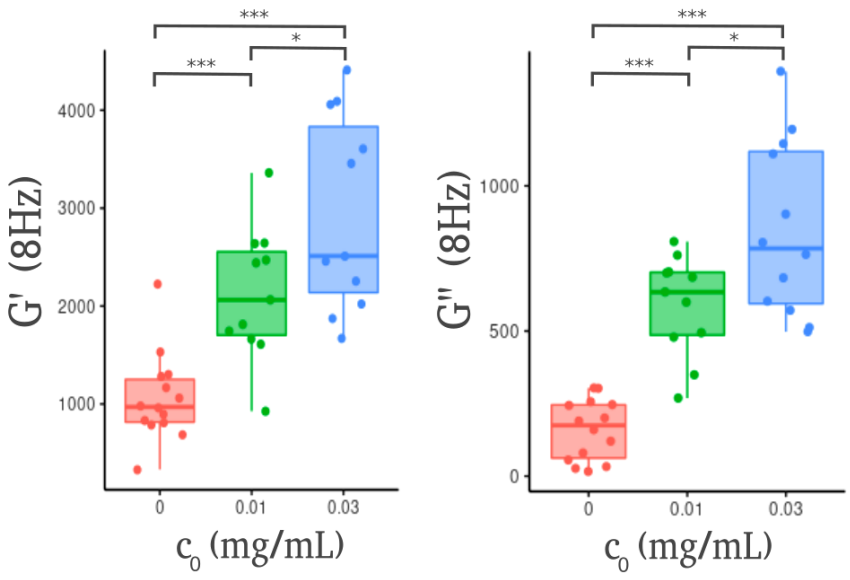


Figure 5: Statistical significance showing differences in moduli $G'$ and $G''$ (in Pa) at 8 Hz. ANOVA test was carried out as explained in §2.5. * $p < 0.05$, ** $p < 0.01$, *** $p < 0.001$.

decreases ($b = -0.05$) then increases ($c = 1$) at higher frequencies.

- $c_0 = 0.01$ and 0.03 mg/mL: $G'$ increases with $f$ ($a = 0.12$) like in a glassy regime (Sollich et al. (1997)). $G''$ does the same ($b = 0.12$) but changes to a slope $c = 1$ at higher frequencies. Exponents $a$ are similar for both $c_0$, but there is reinforcement (larger $G'$ and $G''$) for the larger concentration $c_0 = 0.03$ mg/mL.

- The rheology of used Col-I solutions has been measured using classical rheometry (Anton Paar, model MCR 301, cone–plate geometry, diameter 5 cm, cone angle 0.5°, T=37°C). We found $\eta_0 = 0.8$ mPa.s, $\eta_{0.01} = 0.99\ \mathrm{f}^{-0.044}$ mPa.s and $\eta_{0.03} = 9.1\ \mathrm{f}^{-0.46}$ mPa.s (constant shear rate $\dot{\gamma} = 2\pi\mathrm{f}$, 10 Hz < f < 100 Hz). This shows a Newtonian behavior for culture medium, and non-Newtonian effects for Col-I solutions. These effects are not sufficient to explain

changes in spheroid rheology.

- Static moduli were found : $E_0$ = 3.1 ± 0.7 kPa, $E_{0.01}$ = 3.6 ± 0.9 kPa and $E_{0.03}$ = 5.4 ± 1.3 kPa. They correspond roughly to 3 $G_0$ for incompressible materials, the difference comes from $G_0$, obtained at 1 Hz, rather than in the limit $f \to 0$.

### *3.2. Confocal microscopy*

Confocal images were acquired as described in §2.4. Images taken from Z–stacks were averaged to represent cells within spheroids and Col-I. Three typical images of such spheroids are shown in Figure 6. It can be seen (Figure 6b–c) that Col-I accumulated within the spheroid. Spheroids with Col-I looked more compact with cells firmly embedded within the matrix. On the other hand, spheroids without Col-I seemed to lack cohesion, with cells spreading towards the outside (see also Figure 2, $c_0$ = 0 mg/mL). These effects, together with the measurements of dynamic moduli, will be discussed in the next part.

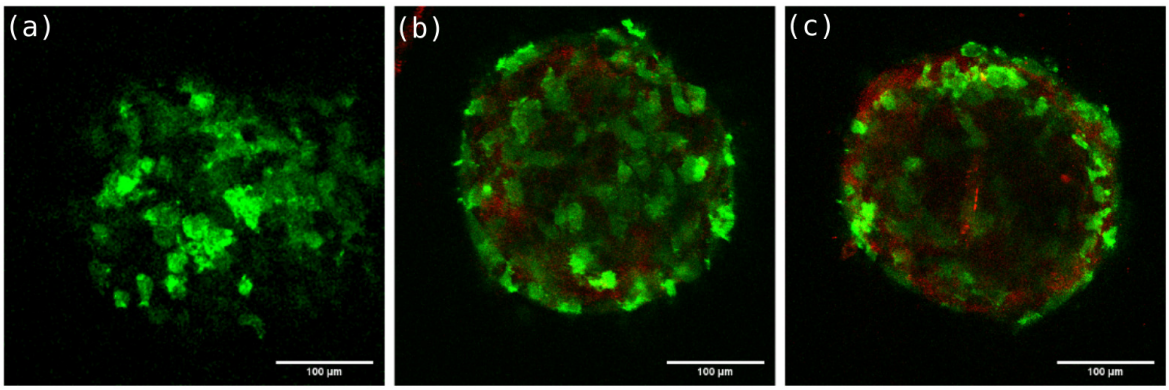


Figure 6: Confocal microstructure of spheroids without or with Col-I. Actin-GFP labeled cells appear in green, whereas Col-I, imaged by reflectance is shown in red. (a) $c_0$=0 (b) $c_0$=0.01mg/mL (c) $c_0$=0.03 mg/mL of Col-I. Scale bar = 100 $\mu$m (same for the three images). Images are projections of 5 slices located at the mid–plane.

## 4. Discussion

Multicellular spheroids are considered as good tumor models, although their mechanical properties remain insufficiently explored. Still these properties are essential to understand the tumor–stroma interactions (Provenzano et al. (2006); Kai et al. (2019); Natarajan et al. (2019)). Interesting works applying osmotic pressures are available (Delarue et al. (2013)) with simultaneous measurements of local stresses within spheroids (Dolega et al. (2017)). Global properties have been measured (Marmottant et al. (2009); Ouchi et al. (2019); Tietze et al. (2019)) in compression or AFM tests, and elegant techniques using Brillouin light scattering are available (Mahajan et al. (2021); Yan et al. (2022)). But there is still a lack regarding general rheological properties in terms of deformation rates and composition of the spheroids, that could help to develop models further (Preziosi et al. (2010); Dolega et al. (2021); Groetsch et al. (2021)). This is what we analyzed in this work using AFM.

We modified the conventional spheroid preparation technique (Figure 1) using hanging drops (Kuo et al. (2017)), in order to avoid adhesion to the substrate; this allowed to prepare well–controlled spheroids at different Col-I contents (Figure 2). Then we used a previous AFM methodology (Giannetti et al. (2020)) to investigate the spheroids rheology (Figure 3) and obtained viscoelastic data covering three decades in frequency (Figure 4)). The method has already provided interesting differences between biological tissues in healthy or modified conditions, such as chondrocytes–based tissues, cartilages and tendons (Lee et al. (2010); Nia et al. (2013); Connizzo and Grodzinsky (2017)). Our data shows that spheroids that had grown without Col-I presented a classical rheological behavior close to cells (Lekka et al. (1999); Rother et al. (2014); Abidine et al.

(2015); Yubero et al. (2020)) with shear moduli between 500 and 2,000 Pa. $G'$ was almost constant (slope 0.05) whereas $G''$ first decreased, then increased (slope $\sim$ 1) at higher frequencies. On the other hand, when spheroid grew within a Col-I solution, the behavior changed drastically: a larger increase (slope 0.12) was found for $G'$ and $G''$ vs. frequency, with $G''$ increasing faster (slope 1) at high frequencies. More importantly significant differences in viscoelasticity were found between the three types of spheroids (Figure 5), showing the reinforcing role of Col-I within the spheroid. Thus AFM rheology appears as a robust technique of investigation to compare such data.

To predict these rheology features, we used the following model: $G' = G_0\, f^a$, $G'' = G_1\, f^b + G_2\, f^c$. We found that $c = 1$ for all Col-I concentrations and $a = b = 0.12$ for cases with Col-I. For $c_0$=0, $a = 0.05$ and $b = -0.05$ (see Table 1). Finally, the transition frequency $f_T$ (Abidine et al. (2018)) decreases with Col-I content, thus Col-I plays the role of a glassy agent. $f_T$ can be considered as a rheology marker, or similarly the loss tangent $\frac{G''}{G'}$, smaller than 1 at low frequencies, then crossing 1 at $f = f_T$ and increasing further at higher frequencies (Rother et al. (2014)).

The interpretation is novel and brings into play the intriguing role of Col-I. Under such conditions, Col-I is a viscous fluid (with a shear–thinning behavior at 0.03 mg/mL), thus it is unexpected to find different spheroids properties going from elastic–like behavior to glassy states, characterized by constant slopes for $G'$ and $G''$ (Sollich et al. (1997)). The response lies in the microstructure of such spheroids. As observed using confocal microscopy (Figure 6), the Col-I network acts as a backbone to allow cells to bind. Figure 6a shows a spheroid without Col-I, and cells appear not well bound together. This may be due to the fact that T24 cells do not express E–cadherins (Bindels et al. (2000)). On the other hand, a more compact spheroid structure was found when adding Col-I (Figure 2 and Figure 6). This probably comes from a better adhesion of

T24 cells to Col-I. The $\beta_1$-integrin subunit may play a role in T24 cell migration and interactions with Col-I (Heyder et al. (2005)). With the increase of Col-I content (Figure 6), cells spred well and exhibited more pointed protrusions. It was shown previously that T24 cells are able to remodel Col-I – as in viscoplastic systems (Iordan et al. (2010)) – and pull/push fibers to align them (Laforgue et al. (2022)) although the given confocal images resolution was not good enough to see this effect here. T24 cell migration may also be important at early times of spheroid formation (<3 days). But in 3D, there is a competition between adhesion and confinement, therefore it is hard to explain observed spheroids properties by cell migration only. Note that ECM (concentration ~ 15%) has already been pointed out to act as a pressure sensor and a regulator of tumor spheroids (Dolega et al. (2021)). Here it is difficult to estimate the Col-I content (Figure 6) but it enhances the formation of more regular spheroids due to cell–Col-I interactions. Such spheroids containing Col-I exhibit larger $G'$ and $G''$ moduli. The resulting behavior is that of a glassy material (Sollich et al. (1997)), allowing efficient cancer cell dynamics (Abidine et al. (2018)), changing constantly between metastable states, this being in favor of tumor invasion.

## 5. Conclusion

Col-I is therefore an essential component allowing cells to bind and form homogeneous spheroids. AFM microrheology was shown to be a valuable tool allowing to capture these changes due to the presence of Col-I, and a soft rheology model was found suitable to predict such behaviors. Confocal microscopy allowed to go deeper into the spheroids by observing differences in microstructure; this needs to be investigated further to capture the fine interactions between cells and Col-I fibres. Future works should focus on the ability of various bladder cancer cells to form stable spheroids

depending on the amount of E–cadherins, Col-I content and cell invasiveness. This would help to understand how tumors can sense/use the micro–environment to grow in size, and how Col-I deposition can be correlated with the rheological properties.

**Declarations**

**Funding:** C.V. is a member of the LabeX Tec 21 (Investissements d'Avenir: grant agreement No. ANR-11-LABX-0030) and is thankful for the access to the confocal microscope facility.

**Acknowledgments:** The authors are thankful to G. Cappello and P. Recho (LIPhy) for valuable discussions regarding this work.

**Availability of data and material:** All the relevant data are available upon request.

## Declaration of Competing Interest

The authors declare that they have no known competing financial interests or personal relationships that could have appeared to influence the work reported in this paper.

## References

Abidine, Y., Constantinescu, A., Laurent, V.M., Rajan, V.S., Michel, R., Laplaud, V., Duperray, A., Verdier, C., 2018. Mechanosensitivity of cancer cells in contact with soft substrates using AFM. Biophys. J. 114, 1165–1175.

Abidine, Y., Giannetti, A., Revilloud, J., Laurent, V.M., Verdier, C., 2021. Viscoelastic properties in cancer: from cells to spheroids. Cells 10, 1704.

Abidine, Y., Laurent, V.M., Michel, R., Duperray, A., Verdier, C., 2015. Local mechanical properties of bladder cancer cells measured by AFM as a signature of metastatic potential. Eur. Phys. J. Plus 130, 202.

Alcaraz, J., Buscemi, L., Grabulosa, M., Trepat, X., Fabry, B., Farré, R., Navajas, D., 2003. Microrheology of human lung epithelial cells measured by atomic force microscopy. Biophys. J. 84, 2071–2079.

Alcaraz, J., Buscemi, L., de Morales, M.P., Colchero, J., Baro, A., Navajas, D., 2002. Correction of microrheological measurements of soft samples with atomic force microscopy for the hydrodynamic drag on the cantilever. Langmuir 18, 716–721.

Bindels, E.M., Vermey, M., van den Beemd, R., Dinjens, W.N., Kwast, T.H.V.D., 2000. E-cadherin promotes intraepithelial expansion of bladder carcinoma cells in an in vitro model of carcinoma in situ. Cancer Res. 60, 177–183.

Brooks, M., Mo, Q., Krasnow, R., Ho, P.L., Lee, Y.C., Xiao, J., Kurtova, A., Lerner, S., Godoy, G., Jian, W., Castro, P., Chen, F., Rowley, D., Ittmann, M., Chan, K.S., 2016. Positive association of collagen type I with non-muscle invasive bladder cancer progression. Oncotarget 7, 82609–82619.

Butt, H.J., Jaschke, M., 1995. Calculation of thermal noise in atomic force microscopy. Nanotechnology 6, 1–7.

Cai, P., Mizutani, Y., Tsuchiya, M., Maloney, J.M., Fabry, B., Vliet, K.J.V., Okajima, T., 2013. Quantifying cell-to-cell variation in power-law rheology. Biophys. J. 105, 1093–1102.

Connizzo, B.K., Grodzinsky, A.J., 2017. Tendon exhibits complex poroelastic behavior at the nanoscale as revealed by high-frequency AFM-based rheology. J. Biomech. 54, 11–18.

Cross, S.E., Jin, Y.S., Rao, J., Gimzewski, J.K., 2007. Nanomechanical analysis of cells from cancer patients. Nat. Nanotechnol. 2, 780–783.

Delarue, M., Montel, F., Caen, O., Elgeti, J., Siaugue, J.M., Vignjevic, D., Prost, J., Joanny, J.F., Cappello, G., 2013. Mechanical control of cell flow in multicellular spheroids. Phys. Rev. Letters 110.

Delarue, M., Montel, F., Vignjevic, D., Prost, J., Joanny, J.F., Cappello, G., 2014. Compressive stress inhibits proliferation in tumor spheroids through a volume limitation. Biophys. J. 107, 1821–1828.

Dolega, M., Zurlo, G., Goff, M.L., Greda, M., Verdier, C., Joanny, J.F., Cappello, G., Recho, P., 2021. Mechanical behavior of multi-cellular spheroids under osmotic compression. J. Mech. Phys. Solids 147, 104205.

Dolega, M.E., Delarue, M., Ingremeau, F., Prost, J., Delon, A., Cappello, G., 2017. Cell-like pressure sensors reveal increase of mechanical stress towards the core of multicellular spheroids under compression. Nat. Comm. 8, 14056.

Fabry, B., Maksym, G.N., Butler, J.P., Glogauer, M., Navajas, D., Fredberg, J.J., 2001. Scaling the microrheology of

living cells. Phys. Rev. Lett. 87, 148102.

Friedl, P., Borgmann, S., Bröcker, E.B., 2001. Amoeboid leukocyte crawling through extracellular matrix: lessons from the dictyostelium paradigm of cell movement. J. Leukoc. Biol. 70, 491–509.

Fung, Y.C., 1993. Biomechanics. Mechanical properties of living tissues. Springer-Verlag, New York.

Giannetti, A., Revilloud, J., Verdier, C., 2020. Mechanical properties of 3D tumor spheroids measured by AFM. Comput. Meth. Biomech. Biomed. Eng. 23, S125–127.

Groetsch, A., Zysset, P.K., Varga, P., Pacureanu, A., Peyrin, F., Wolfram, U., 2021. An experimentally informed statistical elasto-plastic mineralised collagen fibre model at the micrometre and nanometre lengthscale. Sci. Rep. 11, 1–22.

Helmlinger, G., Netti, P.A., Lichtenbeld, H.C., Melder, R.J., Jain, R.K., 1997. Solid stress inhibits the growth of multicellular tumor spheroids. Nat. Biotechnol. 15, 778–783.

Heyder, C., Gloria-Maercker, E., Hatzmann, W., Niggemann, B., Zänker, K.S., Dittmar, T., 2005. Role of the $\beta$1-integrin subunit in the adhesion, extravasation and migration of T24 human bladder carcinoma cells. Clin. Exp. Metastasis 22, 99–106.

Iordan, A., Duperray, A., Gérard, A., Grichine, A., Verdier, C., 2010. Breakdown of cell-collagen networks through collagen remodeling. Biorheology 47, 277–295.

Iordan, A., Duperray, A., Verdier, C., 2008. Fractal approach to the rheology of concentrated cell suspensions. Phys. Rev. E 77, 011911.

Kai, F., Drain, A.P., Weaver, V.M., 2019. The extracellular matrix modulates the metastatic journey. Dev. Cell 49, 332–346.

Kuo, C.T., Wang, J.Y., Lin, Y.F., Wo, A.M., Chen, B.P.C., Lee, H., 2017. Three-dimensional spheroid culture targeting versatile tissue bioassays using a PDMS-based hanging drop array. Sci. Rep. 7, 4363.

Laforgue, L., Fertin, A., Usson, Y., Verdier, C., Laurent, V.M., 2022. Efficient deformation mechanisms enable invasive cancer cells to migrate faster in 3D collagen networks. Sci. Rep. 12, 7867.

Lee, B., Han, L., Frank, E.H., Chubinskaya, S., Ortiz, C., Grodzinsky, A.J., 2010. Dynamic mechanical properties of the tissue-engineered matrix associated with individual chondrocytes. J. Biomech. 43, 469–476.

Lekka, M., Laidler, P., Gil, D., Lekki, J., Stachura, Z., Hrynkiewicz, A.Z., 1999. Elasticity of normal and cancerous human bladder cells studied by scanning force microscopy. Eur. Biophys. J. 28, 312–316.

Levental, I., Georges, P.C., Janmey, P.A., 2007. Soft biological materials and their impact on cell function. Soft Matter 3, 299–306.

Mahajan, V., Beck, T., Gregorczyk, P., Ruland, A., Alberti, S., Guck, J., Werner, C., Schlüßler, R., Taubenberger, A.V., 2021. Mapping tumor spheroid mechanics in dependence of 3D microenvironment stiffness and degradability by Brillouin microscopy. Cancers 13, 5549.

Marmottant, P., Mgharbel, A., Käfer, J., Audren, B., Rieu, J.P., Vial, J.C., van der Sanden, B., Marée, A.F.M., Graner, F., Delanoë-Ayari, H., 2009. The role of fluctuations and stress on the effective viscosity of cell aggregates. Proc. Natl Acad. Sci. USA 106, 17271–17275.

Mierke, C.T., 2019. The matrix environmental and cell mechanical properties regulate cell migration and contribute to the invasive phenotype of cancer cells. Rep. Prog. Phys. 82, 064602.

Natarajan, S., Foreman, K.M., Soriano, M.I., Rossen, N.S., Shehade, H., Fregoso, D.R., Eggold, J.T., Krishnan, V., Dorigo, O., Krieg, A.J., Heilshorn, S.C., Sinha, S., Fuh, K.C., Rankin, E.B., 2019. Collagen remodeling in the hypoxic tumor-mesothelial niche promotes ovarian cancer metastasis. Cancer Res. 79, 2271–2284.

Netti, P.A., Roberge, S., Boucher, Y., Baxter, L.T., Jain, R.K., 1996. Effect of transvascular fluid exchange on pressure-flow relationship in tumors: a proposed mechanism for tumor blood flow heterogeneity. Microvasc. Res. 52, 27–46.

Nia, H., Bozchalooi, I., Li, Y., Han, L., Hung, H.H., Frank, E., Youcef-Toumi, K., Ortiz, C., Grodzinsky, A., 2013. High-bandwidth AFM-based rheology reveals that cartilage is most sensitive to high loading rates at early stages of impairment. Biophys. J. 104, 1529–1537.

Ouchi, R., Togo, S., Kimura, M., Shinozawa, T., Koido, M., Koike, H., Thompson, W., Karns, R.A., Mayhew, C.N., McGrath, P.S., McCauley, H.A., Zhang, R.R., Lewis, K., Hakozaki, S., Ferguson, A., Saiki, N., Yoneyama, Y., Takeuchi, I., Mabuchi, Y., Akazawa, C., Yoshikawa, H.Y., Wells, J.M., Takebe, T., 2019. Modeling steatohepatitis in humans with pluripotent stem cell-derived organoids. Cell metabolism 30, 374–384.

Palade, L.I., Vernay, V., Attané, P., 1996. A modified fractional model to describe the entire viscoelastic behavior of

polybutadienes from flow to glassy regime. Rheol. Acta 35, 265–273.

Plodinec, M., Loparic, M., Monnier, C.A., Obermann, E.C., Zanetti-Dallenbach, R., Oertle, P., Hyotyla, J.T., Aebi, U., Bentires-Alj, M., Lim, R.Y.H., Schoenenberger, C.A., 2012. The nanomechanical signature of breast cancer. Nat. Nanotechnol. 7, 757–765.

Preziosi, L., Ambrosi, D., Verdier, C., 2010. An elasto-visco-plastic model of cell aggregates. J. Theor. Biol. 262, 35–47.

Provenzano, P.P., Eliceiri, K.W., Campbell, J.M., Inman, D.R., White, J.G., Keely, P.J., 2006. Collagen reorganization at the tumor-stromal interface facilitates local invasion. BMC Medicine 4, 38.

Quarto, G., Spinelli, L., Pifferi, A., Torricelli, A., Cubeddu, R., Abbate, F., Balestreri, N., Menna, S., Cassano, E., Taroni, P., 2014. Estimate of tissue composition in malignant and benign breast lesions by time-domain optical mammography. Biomed. Opt. Express 5, 3684–3698.

Riedl, J., Crevenna, A.H., Kessenbrock, K., Yu, J.H., Neukirchen, D., Bista, M., Bradke, F., Jenne, D., Holak, T.A., Werb, Z., Sixt, M., Wedlich-Soldner, R., 2008. Lifeact: a versatile marker to visualize F-actin. Nat. Methods 5, 605–607.

Rother, J., Nöding, H., Mey, I., Janshoff, A., 2014. Atomic force microscopy-based microrheology reveals significant differences in the viscoelastic response between malign and benign cell lines. Open Biology 4, 140046.

Sollich, P., Lequeux, F., Hébraud, P., Cates, M.E., 1997. Rheology of soft glassy materials. Phys. Rev. Letters 78, 2020–2023.

Stamenovic, D., Rosenblatt, N., Montoya-Zavala, M., Matthews, B.D., Hu, S., Suki, B., Wang, N., Ingber, D.E., 2007. Rheological behavior of living cells is timescale-dependent. Biophys. J. 93, L39–L41.

Tietze, S., Kräter, M., Jacobi, A., Taubenberger, A., Herbig, M., Wehner, R., Schmitz, M., Otto, O., List, C., Kaya, B., Wobus, M., Bornhäuser, M., Guck, J., 2019. Spheroid culture of mesenchymal stromal cells results in morphorheological properties appropriate for improved microcirculation. Adv. Sci. 6, 1900622.

Trepat, X., Lenormand, G., Fredberg, J.J., 2008. Universality in cell mechanics. Soft Matter 4, 1750–1759.

Verdier, C., Etienne, J., Duperray, A., Preziosi, L., 2009. Review: Rheological properties of biological materials. C. R. Acad. Sci. Phys. 10, 790–811.

Weiswald, L.B., Bellet, D., Dangles-Marie, V., 2015. Spherical cancer models in tumor biology. Neoplasia 17, 1–15.

Whatcott, C.J., Diep, C.H., Jiang, P., Watanabe, A., LoBello, J., Sima, C., Hostetter, G., Shepard, H.M., Von Hoff, D.D., Han, H., 2015. Desmoplasia in primary tumors and metastatic lesions of pancreatic cancer. Clin. Cancer Res. 21, 3561–3568.

Xu, S., Xu, H., Wang, W., Li, S., Li, H., Li, T., Zhang, W., Yu, X., Liu, L., 2019. The role of collagen in cancer: from bench to bedside. J. Transl. Med. 17, 309.

Yan, G., Monnier, S., Mouelhi, M., Dehoux, T., 2022. Probing molecular crowding in compressed tissues with Brillouin light scattering. Proc. Natl Acad. Sci. USA 119, e2113614119.

Yubero, M.L., Kosaka, P.M., San Paulo, A., Malumbres, M., Calleja, M., Tamayo, J., 2020. Effects of energy metabolism on the mechanical properties of breast cancer cells. Commun. Biology 3, 590.